Ligand Preferences of Kringle 2 and Homologous Domains of Human Plasminogen: Canvassing Weak, Intermediate, and High-Affinity Binding Sites by ^{1}H-NMR†

Daniel N. Marti,‡ Chih-Kao Hu,‡ Seong Soo A. An,‡ Priska von Haller,§ Johann Schaller,§ and Miguel Llinás*,‡

Department of Chemistry, Carnegie Mellon University, Pittsburgh, Pennsylvania 15213, and Department of Chemistry and Biochemistry, University of Bern, CH-3012 Bern, Switzerland

Received June 2, 1997; Revised Manuscript Received July 21, 1997⊗

ABSTRACT: The interaction of various small aliphatic and aromatic ionic ligands with the human plasminogen (HPg) recombinant kringle 2 (r-K2) domain has been investigated by ^{1}H-NMR spectroscopy at 500 MHz. The results are compared against ligand-binding properties of the homologous, lysine-binding HPg kringle 1 (K1), kringle 4 (K4), and kringle 5 (K5). The investigated ligands include the ω-aminocarboxylic acids 4-aminobutyric acid (4-ABA), 5-aminopentanoic acid (5-APA), 6-aminohexanoic acid (6-AHA), 7-aminoheptanoic acid (7-AHA), lysine and arginine derivatives with free and blocked α-amino and/or carboxylate groups, and a number of cyclic analogs, zwitterions of similar size such as *trans*-(aminomethyl)-cyclohexanecarboxylic acid (AMCHA) and *p*-benzylaminesulfonic acid (BASA), and the nonzwitterions benzylamine and benzamidine. Equilibrium association constant (K_a) values were determined from ^{1}H-NMR ligand titration profiles. Among the aliphatic linear ligands, 5-APA ($K_a \sim 3.4$ mM^{-1}) shows the strongest interaction with r-K2 followed by 6-AHA ($K_a \sim 2.3$ mM^{-1}), 7-AHA ($K_a \sim 0.45$ mM^{-1}), and 4-ABA ($K_a \sim 0.22$ mM^{-1}). In contrast, r-K1, K4, and K5 exhibit a preference for 6-AHA ($K_a \sim 74.2$, 21.0, and 10.6 mM^{-1}, respectively), a ligand ∼1.14 Å longer than 5-APA. Mutations R220G and E221D increase the affinity of r-K2 for these ligands but leave the selectivity profile essentially unaffected: 5-APA > 6-AHA > 7-AHA > 4-ABA ($K_a \sim 6.5$, 3.9, 1.8, and 0.74 mM^{-1}, respectively). We find that, while r-K2 definitely interacts with N^{α}-acetyl-L-lysine and L-lysine ($K_a \sim 0.96$ and 0.68 mM^{-1}, respectively), the affinity for analogs carrying a blocked carboxylate group is relatively weak ($K_a \sim 0.1$ mM^{-1}). We also investigated the interaction of r-K2 with L-arginine ($K_a \sim 0.31$ mM^{-1}) and its derivatives N^{α}-acetyl-L-arginine ($K_a \sim 0.55$ mM^{-1}), N^{α}-acetyl-L-arginine methyl ester ($K_a \sim 0.07$ mM^{-1}), and L-arginine methyl ester ($K_a \sim 0.03$ mM^{-1}). Zwitterionic γ-guanidinobutyric acid, containing one less methylene group than arginine, exhibits a K_a of ∼0.28 mM^{-1}. The affinity of r-K2 for lysine and arginine derivatives suggests that K2 could play a role in intermolecular as well as intramolecular interactions of HPg. As is the case for the HPg K1, K4, and K5, among the tested ligands, AMCHA is the one which interacts most firmly with r-K2 ($K_a \sim 7.3$ mM^{-1}) while the aromatic ligands BASA, benzylamine, and benzamidine exhibit K_a values of ∼4.0, ∼0.04, and ∼0.03 mM^{-1}, respectively. The relative stability of these interactions indicates a strict requirement for *both* cationic and anionic polar groups in the ligand, whereas the presence of a lipophilic aromatic group seems to be of lesser consequence. Ligand-induced shifts of r-K2 ^{1}H-NMR signals and two-dimensional nuclear Overhauser effect (NOESY) experiments in the presence of 6-AHA reveal direct involvement of residues Tyr^{36}, Trp^{62}, Phe^{64}, and Trp^{72} (kringle residue numbering convention) in ligand binding. Starting from the X-ray crystallographic structure of HPg K4 and the intermolecular ^{1}H-NMR NOE data, two models of the K2 lysine binding site complexed to 6-AHA have been derived which differ mainly in the extent of electrostatic pairing between the K2 Arg^{56} and Glu^{57} side chains. Competition between these two conformations in equilibrium may account for the relatively lesser affinity of the K2 domain for zwitterionic lysine-type ligands.

Human plasminogen (HPg),[1] the inert precursor of plasmin, is a single-chain protein of 791 amino acids (Sottrup-Jensen et al., 1978; Forsgren et al., 1987). Reflecting heterogeneous glycosylation, it occurs as two main variants with M_r values of ∼ 92 and ∼ 90 kDa (Wiman, 1977; Hayes & Castellino, 1979a,b). The molecule is composed as a mosaic structure which includes the N-terminal peptide (M_r ∼ 9 kDa), five kringle modules (each with an M_r of ∼9 kDa), and a serine protease catalytic unit ($M_r \sim 25$ kDa). Kallikrein, tissue-type HPg activator (tPA), and urokinase-type HPg activator (uPA) cleave HPg at the Arg^{561}−Val^{562} peptide bond, thus resulting in the proteolytically active plasmin which, in turn, is responsible for the degradation of the fibrin matrix of blood clots.

Kringle domains are present in a variety of other proteins of the fibrinolytic and blood coagulation system such as tPA (Pennica et al., 1983), uPA (Günzler et al., 1982), prothrombin (PT) (Magnusson et al., 1975), and coagulation factor XII (McMullen & Fujikawa, 1985). The five kringles of

† This research was supported by NIH Grant HL-29409 from the U.S. Public Health Service and Grants 31-32357.91 and 31-39298.93 from the Swiss National Science Foundation.

* Author to whom correspondence should be addressed.
‡ Carnegie Mellon University.
§ University of Bern.

⊗ Abstract published in *Advance ACS Abstracts,* September 1, 1997.

S0006-2960(97)01316-0 CCC: $14.00

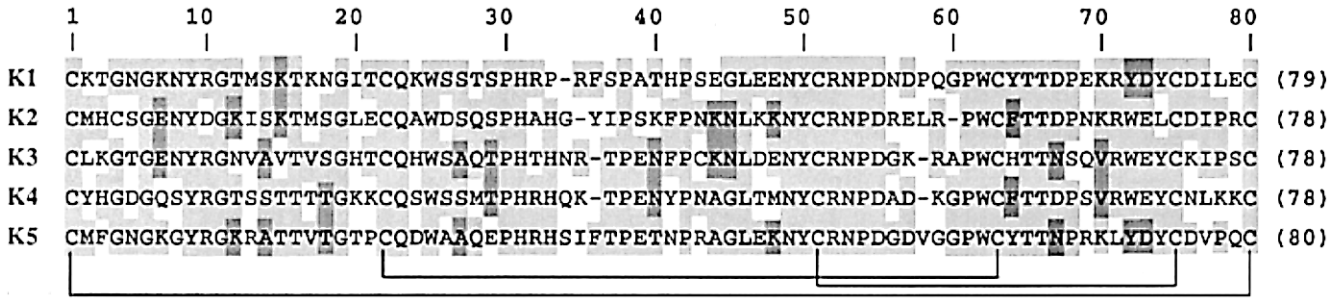

FIGURE 1: Sequence alignment of the five human plasminogen kringles. Amino acids are numbered according to the standard kringle residue numbering convention (Llinás et al., 1983; Tulinsky et al., 1988b). Conserved cystines (Cys pairs 1 and 80, 22 and 63, and 51 and 75) are indicated under the K5 sequence, which serves as a template for the alignment. The total number of amino acids for each kringle is given (in parentheses). Conserved residues in two or more kringles are highlighted by two grades of shading. For the NMR studies, a $Cys^4 \rightarrow$ Gly mutation was introduced in r-K2 to avoid dimerization.

HPg contain between 78 and 80 amino acids each, with ~35% sequence identity (Figure 1). The kringle structure is shaped by a characteristic 1−6, 2−4, 3−5 disulfide bond pattern involving six conserved Cys residues in positions[2] 1, 22, 51, 63, 75, and 80. The orientation of the HPg kringle 2 (K2) relative to the kringle 3 (K3) is restricted by an interkringle disulfide bridge that connects Cys^4 in K2 to Cys^{43} in K3. Solution structures of HPg kringle 1 (K1) (Rejante & Llinás, 1994a), human and equine plasminogen kringle 4 (K4) (Atkinson & Williams, 1990; Cox et al., 1994), tPA kringle 2 (Byeon & Llinás, 1991), and the uPA kringle (Li et al., 1994; Hansen et al., 1994) have been determined by ^{1}H-NMR. Independently, X-ray crystallographic structures have been obtained for HPg K1 (Wu et al., 1994; Mathews et al., 1996), HPg K4 (Mulichak et al., 1991; Wu et al., 1991), tPA kringle 2 (de Vos et al., 1992), PT kringle 1 (Tulinsky et al., 1988a), and PT kringle 2 (Arni et al., 1993). The X-ray structure of the 36th K4-type kringle of apolipoprotein (a) has also been reported (Mikol et al., 1996).

Kringle domains are thought to impart binding specificity to their parent proteins. Thus, to a large extent, the affinity of HPg and tPA for fibrin is thought to be founded on the interaction of particular kringle domains with lysine side chains exposed by the fibrin matrix. Similarly, a relaxed conformation and increased activation rate of recombinant HPg are likely to result from intramolecular interactions which are disrupted by amino acid mutations affecting the lysine binding sites of K1, K4, or K5 (Menhart et al., 1995; McCance & Castellino, 1995). Furthermore, human angiostatin, which comprises the HPg K1−K4 segment of HPg, is a potent inhibitor of angiogenesis (O'Reilly et al., 1994; Cao et al., 1996).

Markus et al. (1979) first detected the presence of approximately one high-affinity and approximately five low-affinity ω-aminocarboxylic acid binding sites in HPg. However, to this date, the precise location of such sites and their significance according to the tested ligand have not been fully characterized. In the case of HPg, zwitterionic ligands such as 6-aminohexanoic acid (6-AHA) measurably interact with K1 (Lerch et al., 1980; De Marco et al., 1982; Motta et al., 1987; Menhart et al., 1991; Rejante, 1992), K2 (Marti et al., 1994; Söhndel et al., 1996), K4 (Hochschwender et al., 1983; Rejante et al., 1991; Rejante, 1992; McCance et al., 1994), and K5 (Thewes et al., 1990; McCance et al., 1994), whereas K3 apparently lacks a functional binding site for such ligands (Marti et al., 1994; Söhndel et al., 1996). The above-mentioned ^{1}H-NMR, X-ray crystallographic, and mutant gene expression studies have led to the identification of key residues participating in ligand binding by K1, K4, and K5. The consensus model (Tulinsky et al., 1988a) places the ligand carboxylate group undergoing ionic interaction with Arg^{71} (and possibly Arg^{35}/Lys^{35}), while the distal amino group of the same ligand molecule ion-pairs the anionic side chains of Asp^{55} and Asp^{57}. Ligand binding is further stabilized via van der Waals interactions of ligand hydrocarbon backbone groups with hydrophobic side chains such as those exposed by Phe^{36}, Trp^{62}, Tyr^{64} and Tyr^{72} in K1, Trp^{62}, Phe^{64} and Trp^{72} in K4, and Phe^{36}, Trp^{62}, Tyr^{64} and Tyr^{72} in K5.

In this paper, we report a first, comprehensive ^{1}H-NMR characterization of the ligand binding properties of HPg K2. The study includes linear zwitterionic ligands, lysine and arginine derivatives, and cyclic aliphatic as well as aromatic ligands. Results are compared with new and previous ^{1}H-NMR data obtained in our laboratories on HPg K1, K4, and K5, respectively (Thewes et al., 1990; Rejante et al., 1991; Rejante, 1992). In addition, the cloning and expression of

[1] Abbreviations: 2D, two-dimensional; 4-ABA, 4-aminobutyric acid; 5-APA, 5-aminopentanoic acid; 6-AHA, 6-aminohexanoic acid; 7-AHA, 7-aminoheptanoic acid; AcArg, N^{α}-acetyl-L-arginine; AcArgME, N^{α}-acetyl-L-arginine methyl ester; AcLys, N^{α}-acetyl-L-lysine; AcLysME, N^{α}-acetyl-L-lysine methyl ester; AMCHA, *trans*-(aminomethyl)cyclohexanecarboxylic acid; Arg, L-arginine; ArgME, L-arginine methyl ester; BASA, *p*-benzylaminesulfonic acid; bp, base pair; COSY, 2D chemical shift correlated spectroscopy; DTT, 1,4-dithio-DL-threitol; FXa, activated coagulation factor X; γ-GBA, γ-guanidinobutyric acid; HPg, human plasminogen; K1, kringle 1 domain of HPg (Cys^{84}−Cys^{162}), generated as r-K1; K2, kringle 2 domain of HPg (Cys^{166}−Cys^{243}), generated as r-K2; K3, kringle 3 domain of HPg (Cys^{256}−Cys^{333}); K4, kringle 4 domain of HPg (Cys^{358}−Cys^{435}), generated as fragment Val^{355}−Ala^{440} (Val^{442}) of HPg; K5, kringle 5 domain of HPg (Cys^{462}−Cys^{541}), generated as fragment Val^{449}−Phe^{546} of HPg; K35Y*, substitution $Lys^{35} \rightarrow$ Tyr in K4, based on the kringle sequence alignment (Figure 1) where Lys^{35} of K4 corresponds to Tyr^{36} in the K2 sequence; K_a, equilibrium association constant; *l*, dipole length; Lys, L-lysine; LysME, L-lysine methyl ester; NOE, nuclear Overhauser effect; NOESY, 2D NOE correlated spectroscopy; PCR, polymerase chain reaction; pH*, glass electrode pH reading, uncorrected for the deuterium isotope effect; PT, human prothrombin; r-K1, recombinant HPg fragment K77M/KVYLSE-[K1]EE containing mutation K77M, where the fragment is reduced to the sequence YLSE[K1]EE after elastase cleavage; r-K2, recombinant HPg fragment C162T/E163S/EE[K2/C169G]T containing mutations C162T, E163S, and C169G; r-K2mut, recombinant HPg fragment C162T/E163S/EE[K2/C169G/R220G/E221D]T containing mutations C162T, E163S, C169G, R220G, and E221D and an attached N-terminal hexahistidine tag (MRGSHHHHHHGSIEGR); RT, room temperature; TOCSY, 2D total correlation spectroscopy; tPA, human tissue-type plasminogen activator; uPA, human urokinase-type plasminogen activator.

[2] Kringle residues are numbered according to the standard kringle numbering convention (Figure 1). However, when protein expression and vector constructs are referred to, numbering is by reference to the Glu^1-plasminogen sequence (Forsgren et al., 1987).

recombinant HPg K1 (r-K1), K2 (r-K2), and a K2 mutant (r-K2mut) are reported. The latter, incorporating mutations R56G and E57D at the binding site, was investigated in order to probe the functional (ligand binding) significance of the conservative $Asp^{57} \rightarrow Glu$ substitution that distinguishes the wild-type K2 from other lysine-binding kringles in HPg. Structural models of the K2 binding site based on the crystallographic structure of HPg K4 (Mulichak et al., 1991) and intermolecular ^{1}H-NMR Overhauser data for the r-K2 in the presence of 6-AHA are discussed.

EXPERIMENTAL PROCEDURES

Plasmids and Bacterial Strains. Vectors pAR3038 and pMa5-8 were used to express r-K1 as a nonfusion protein. pAR3038 includes the bacteriophage T7 promoter *ϕ10*, the gene *10* translation start site s*10*, the transcription terminator T*ϕ*, and a *β*-lactamase selectable marker (Rosenberg et al., 1987). Vector pMa5-8 contains a ColE1-type and f1-type origin of replication and the *β*-lactamase gene (Stanssens et al., 1989). Plasmid pQE-8 utilized for the expression of r-K2 and r-K2mut was obtained from Qiagen. The vector contains the regulatable *Escherichia coli* bacteriophage T5 promoter/*lac* operator element N250PSN250P29, a synthetic ribosomal binding site RBS II, and the phage *λ* transcription terminator t_o, encodes *β*-lactamase, and fuses an N-terminal hexahistidine tag to the recombinant protein (Hochuli et al., 1988). Plasmid pREP4 (Qiagen) expresses elevated levels of the *lac* repressor and confers kanamycin resistance. Plasmid pPLGKG (Forsgren et al., 1987) carrying the cDNA sequence of HPg was a kind gift of Prof. L.-O. Hedén (University of Lund, Lund, Sweden). High-level expression of r-K2/r-K2mut and r-K1 was achieved in *E. coli* strains BL21 and BL21(DE3) (F^- *ompT* r_B^- m_B^-), respectively (Studier et al., 1990). *E. coli* strain HB101 was employed for routine transformations and plasmid preparations.

Construction of the Expression Vector for r-K77M/KVYLSE[K1]EE (r-K1). The cDNA fragment corresponding to the HPg sequence Lys^{78}−Glu^{164} was amplified from pPLGKG by polymerase chain reaction (PCR). The PCR 5′-primer 5′-ggcagcAt**AtG**AAAGTGTATCTCTCA-3′, complementary to a segment of the noncoding HPg cDNA, was employed to introduce a *Nde*I restriction endonuclease site upstream of the codon for Lys^{78}. Through insertion of the *Nde*I restriction site, the codon for Lys^{77} was altered to the translation start codon ATG (bold type) encoding Met. The PCR 3′-primer 3′-GAACTCACACTTCTC**aTc**gtATACtcgAg-5′, which interacts within a region of the coding strand of the HPg cDNA, was used to introduce a stop codon (bold type) and *Nde*I restriction endonuclease site downstream of the codon for Glu^{164}. The K1 PCR product was cloned into the *Eco*RV restriction site of vector pBR322, and both strands of the insert were sequenced. Following cleavage by *Nde*I, the K1 cDNA was inserted into the single *Nde*I restriction site of expression vector pAR3038. The direction of the insert was determined by *Pst*I digestion generating a DNA fragment of either ∼1380 or ∼1460 bp. From the K1−pAR3038 construct, an ∼711 bp DNA segment containing the T7 promoter (*ϕ10*), the gene 10 translation start site (s*10*), the K1 cDNA sequence, and the transcription terminator (T*ϕ*) was excised by digestion with *Sph*I and *Eco*RV. The isolated DNA fragment was incubated with the Klenow fragment, ligated into the *Sma*I restriction site of vector pMa5-8, and transformed into *E. coli* strain BL21(DE3) for the expression of r-K1.

Construction of the Expression Vector for r-C162T/E163S/EE[K2/C169G]T (r-K2). The HPg cDNA fragment encoding amino acids Glu^{164}−Thr^{244} was amplified by PCR using plasmid pPLGKG as the DNA template. The PCR 5′-primer 5′-gCggaTcCatCgagggTaga**acTtct**GAGGAATGTATGCAT**gGC**AGTGGAG-3′, complementary to a segment of the noncoding HPg cDNA strand, introduced a *Bam*HI restriction endonuclease site and the codons for a factor Xa sensitive cleavage site I-E-G-R upstream of the codon for Cys^{162}. These insertions were necessary in order to clone the PCR product into pQE-8 and to cleave the N-terminal hexahistidine tail encoded by pQE-8. The PCR 5′-primer also effected mutations C162T, E163S, and C169G (bold type), resulting in an increased efficiency of the factor Xa cleavage and the exchange of Cys^{169}, which participates in the inter-kringle disulfide bond between K2 and K3. The PCR 3′-primer 3′-TAGGGGGCGACGTGT**atTatc**ccTaGgcG-5′, complementary to a fragment of the coding strand of the HPg cDNA, inserted two stop codons (bold type) and a *Bam*HI restriction endonuclease site downstream of the codon for Thr^{244}. For expression, the K2 PCR product was cloned into pQE-8 as described (Marti et al., 1994).

Construction of the Expression Vector for r-C162T/E163S/EE[K2/C169G/R220G/E221D]T (r-K2mut). A method consisting of two successive rounds of PCR (Mikaelian & Sergeant, 1992) was applied to introduce the codons for the R220G and E221D mutations in the K2 cDNA. Besides the PCR 5′- and 3′-primers discussed above, two additional primers, 5′-ggggcccttAAGACCATGTCTGG-3′ and 3′-GCATTGGGGCTA**cCCCTg**GACGCCGGAACC-5′, were required for the generation of the internally altered K2 cDNA fragment. All cloning steps were performed as described (Marti et al., 1994).

Expression of r-K1, r-K2, and r-K2mut. *E. coli* cells were grown in 2×YT medium (containing 50 *μ*g of ampicillin/mL in the case of r-K1 and 100 *μ*g of ampicillin/mL and 25 *μ*g of kanamycin/mL in the case of r-K2 and r-K2mut, respectively) at 37 °C to an A_{600} of about 0.7−0.9. To induce the production of recombinant protein, isopropyl thio-*β*-D-galactopyranoside was added to a final concentration of 0.4 mM (r-K1) and 2 mM (r-K2 and r-K2mut). Cells were grown for an additional 4.5 h at 37 °C and finally harvested by centrifugation for 30 min (4000*g* at 4 °C). The cell paste was stored at −20 °C.

Refolding and Isolation of r-K1. The cell pellet recovered from 12 L of culture was suspended in 50 mM Tris-HCl (pH 8, 5 mL/g of cell paste) containing lysozyme (0.5 mg/mL), deoxyribonuclease I (0.01 mg/mL), and ribonuclease (0.01 mg/mL). The suspension was stirred at 0 °C for 0.5 h, subjected to sonication for 5 min, and stirred for an additional 1 h at 0 °C. The soluble and insoluble fractions were separated by centrifugation for 1 h (10000*g* at 4 °C) and subsequently processed individually. The soluble fraction of the cell lysis step was stirred overnight in the presence of reduced and oxidized glutathione (1.25 mM each) at 4 °C. The solution was dialyzed against 50 mM Tris-HCl (pH 8) and centrifuged for 30 min (10000*g* at 4 °C). Seventy milliliters of lysine−BioGel was added to the supernatant fraction and stirred for 12 h at 4 °C. The lysine−BioGel was recovered in a Büchner funnel and successively washed with 50 mM Tris-HCl (pH 8) containing 500 mM sodium chloride and 50 mM Tris-HCl (pH 8). Bound r-K1 was eluted with 50 mM Tris-HCl (pH 8) containing 200 mM 6-AHA. The eluate was dialyzed against water and lyoph-

ilized. The insoluble fraction of the cell lysis step was suspended in 50 mM Tris-HCl (pH 8) containing 6 M urea and 5 mM DTT and stirred overnight at RT. The suspension was stepwise diluted with 4 volumes of 50 mM Tris-HCl (pH 8) containing reduced and oxidized glutathione (1.25 mM each) and incubated for 6 h at 4 °C. Then, the solution was dialyzed against 50 mM Tris-HCl (pH 8) and centrifuged for 30 min (10000*g* at 4 °C). r-K1 was isolated from the soluble fraction on lysine−BioGel as described above. Further purification of r-K1 was achieved by ion exchange on a Mono Q HR 5/5 (Pharmacia) column by applying a potassium chloride gradient (0 to 200 mM) in 20 mM Tris-HCl (pH 8). Incubation with elastase liberated the N-terminal peptide M^{77}-K-V. Cleavage was performed in 200 mM Tris-HCl (pH 8.8) for 40 min at 37 °C (enzyme to substrate ratio of 1/100, by mass). Finally, r-K1 was purified by gel filtration on a Sephadex G-50f column (2.5 cm × 100 cm).

Isolation, Refolding, and Purification of r-K2 and r-K2mut. Recombinant r-K2 and r-K2mut were isolated by affinity chromatography on a Ni^{2+}−nitrilotriacetic acid−agarose column, refolded, and purified by affinity chromatography on lysine−BioGel as reported (Marti et al., 1994; Söhndel et al., 1996). The hexahistidine tag in r-K2 was cleaved by incubation with FXa for 24 h at 37 °C in 50 mM Tris-HCl (pH 8) containing 100 mM sodium chloride (enzyme to substrate ratio of 1/100, by mass). Final purification of r-K2/r-K2mut was performed by gel filtration on a column of Sephadex G-50f (2.5 cm × 100 cm) equilibrated with 50 mM ammonium bicarbonate.

Isolation of Kringle 4 and Kringle 5. K4 and K5 were prepared via elastase cleavage of HPg and pepsin digestion of mini-plasminogen, respectively, as previously described (Petros et al., 1989; Thewes et al., 1987).

Protein Characterization. Protein sequence and molecular mass analyses were carried out using Edman degradation in a pulsed-liquid-phase sequenator 477A from Applied Biosystems and electrospray mass spectrometry on a VG platform from Micromass, respectively (Marti et al., 1994; Söhndel et al., 1996).

NMR Spectroscopy. Kringle samples were incubated at 37 °C for 3 h in ^2H_2O to exchange labile hydrogen atoms for deuterons. After lyophilization, the exchanged samples were dissolved in 350 μL of ^2H_2O (99.996 at. % ^2H, Isotec Inc.) at a concentration of ∼0.5 mM and the pH* was adjusted to 7.2 by addition of ^2HOAc or NaO^2H. Ligand titration experiments were performed at 25 °C by adding small aliquots of a 30−150 mM stock solution of ligand dissolved in ^2H_2O. ^1H-NMR data (500 MHz) were acquired in the Fourier mode with quadrature detection on a Bruker AM-500 spectrometer. For each titration point, 640−800 transients with a spectral width of 7246 Hz were accumulated with 8K complex points (digital resolution of 0.91 Hz). The residual $^1H^2HO$ signal was suppressed by selective low-power irradiation during the 1 s relaxation delay between scans. Data were processed with the FELIX-2.3 program (Biosym). After zero-filling to 16K complex points, Gaussian multiplication was used for resolution enhancement. Chemical shifts are referred to the sodium 3-(trimethylsilyl)-[2,2,3,3-$^2H_4$]propionate resonance using *p*-dioxane as an internal standard (De Marco, 1977). Phase sensitive COSY spectra (Wider et al., 1984) were recorded for the kringle close to ligand saturation at 37 °C; 400−512 t_1 increments of 2K complex t_2 points were implemented. Low-power $^1H^2HO$ presaturation was applied during the relaxation delay of 0.7 s. The time domain data in t_1 was subjected to linear prediction and zero-filling to 4K points. Sinebell window functions were applied to data along both t_1 and t_2 dimensions. Phase sensitive NOESY spectra (Kumar et al., 1980) of r-K2 in the presence of 6-AHA were acquired with 512 increments in t_1 (2K complex t_2 points) and mixing times of 75, 125, 200, and 300 ms. Forty-five degree-shifted squared sinebell window functions were applied along both dimensions.

Calculation of Equilibrium Association Constants (K_a). Assuming single-site kringle−ligand interaction and fast ligand exchange (De Marco et al., 1987), the fraction of bound kringle is related to the ligand-induced chemical shift as follows:

$$\Delta p = \frac{\delta_{obs} - \delta_{free}}{\delta_{bound} - \delta_{free}} = \frac{[KS]}{[K_o]} \quad (1)$$

where δ_{free} and δ_{bound} represent chemical shifts of selected kringle signals ligand-free and in the presence of a saturating concentration of ligand, respectively, and δ_{obs} corresponds to the observed chemical shift in the course of the titration experiment. [KS] denotes the concentration of ligand-bound kringle, and $[K_o]$ (=[KS] + [K]) is the total kringle concentration. Equation 1 can be fitted to the hyperbolic Langmuir adsorption equation (eq 2) or its linearized form (eq 3) (De Marco et al., 1982)

$$\Delta p = \frac{K_a[S]}{1 + K_a[S]} \quad (2)$$

$$\frac{1}{\Delta p} = 1 + \frac{1}{K_a}\frac{1}{[S_o] - \Delta p[K_o]} \quad (3)$$

where [S] (=$[S_o] - \Delta_p[K_o]$) and $[S_o]$ (=[S] + [KS]) stand for the free and total ligand concentration, respectively, K_a values were calculated by linear least-squares fitting to eq 3, as well as by nonlinear least-squares fitting to eq 2. For the nonlinear fit, eq 2 was substituted by $y = abx/(1 + bx)$, where x corresponds to the calculable concentration [S] of the free ligand and y to Δ_p. Values a and b were generated by the fitting procedure, where $b = K_a$ and $a = \Delta_p$ at saturating ligand concentrations. If ligand saturation was reached in the titration experiment, $a \sim 1$. After a first round of calculations involving data extracted from monitoring four to seven kringle resonances per tested ligand, Δ_p was divided by a and calculations were repeated with the altered Δ_p until the iterative procedure converged. This method allowed us to estimate binding constants as low as ∼0.03 mM^{-1}. Reported K_a's (Table 1) represent values averaged from various binding curves; standard deviations from the average were calculated by taking into account K_a's generated via both the linear and nonlinear fitting protocols.

Molecular Modeling of the K2 Lysine Binding Site. CHARMm-23.1 (Quanta-4.1; Molecular Simulations Inc.) molecular dynamics software (Brooks et al., 1983) was used for the structural calculations (Kaptein et al., 1988) of the K2 binding site complexed to 6-AHA. The 1.9 Å X-ray crystallographic structure of HPg K4 (Mulichak et al., 1991) was used as a template for modeling the K2 binding site by introducing mutations R32A, Q34G, K35Y*, A56R, D57E, and Y74L. The side chains of residues Tyr^{36}, Asp^{55}, Glu^{57}, Arg^{71}, and Leu^{74} were subjected to an adopted-basis Newton

Table 1: Ligand Affinities of Human Plasminogen Kringles: Equilibrium Association Constants (K_a in mM^{-1}) Determined by ^{1}H-NMR Spectroscopy[a]

ligand	r-K1	r-K2	K4	K5
4-aminobutyric acid	5.1 ± 0.6	0.22 ± 0.03	11 ± 1	0.2 ± 0.04
5-aminopentanoic acid	44.6 ± 7	3.4 ± 0.4	16 ± 1[c]	0.72 ± 0.07
6-aminohexanoic acid	74.2 ± 8	2.3 ± 0.2	21 ± 1[c]	10.6 ± 0.2[h]
7-aminoheptanoic acid	13.8 ± 4.1	0.45 ± 0.04	6.6 ± 0.02[c]	2.1 ± 0.2
L-lysine	2.7 ± 0.05[b]	0.68 ± 0.05	24.4 ± 2.5[d]	0.1 ± 0.0[h]
N^{α}-acetyl-L-lysine	41 ± 2[b]	0.96 ± 0.11	37 ± 1[e]	0.18 ± 0.01
L-lysine methyl ester	0.16 ± 0.005[b]	0.10 ± 0.01	1.5 ± 0.3[f]	0.17 ± 0.05
N^{α}-acetyl-L-lysine methyl ester	0.16 ± 0.005[b]	0.10 ± 0.02	0.2 ± 0.0[f]	0.28 ± 0.08
L-arginine	nb[b]	0.31 ± 0.02	nb[c]	nb[h]
N^{α}-acetyl-L-arginine	0.72 ± 0.04	0.55 ± 0.13	0.32 ± 0.02[c]	nb[h]
L-arginine methyl ester	nb	0.03 ± 0.002	nb[c]	0.17 ± 0.03
N^{α}-acetyl-L-arginine methyl ester	0.09 ± 0.01	0.07 ± 0.02	0.08 ± 0.01[c]	nb[h]
γ-guanidinobutyric acid	2.8 ± 0.05[b]	0.28 ± 0.02	2.6 ± 0.4	0.37 ± 0.07
AMCHA	>300[b]	7.3 ± 0.6	159 ± 2[e]	44.2 ± 4.1
BASA	82 ± 6[b]	4 ± 0.3	74[g]	2.2 ± 0.1[h]
benzylamine	0.16 ± 0.04	0.04 ± 0.01	0.18 ± 0.03[c]	6.3 ± 0.5[h]
benzamidine	0.08 ± 0.05	0.03 ± 0.01	nb[c]	3.4 ± 0.1[h]

[a] Ligand titration experiments were performed in ^2H_2O at pH* 7.2 and 25 °C. Unspecific or very weak ligand interactions, undetected in the ^{1}H-NMR experiments (K_a < 0.03 mM^{-1}), are denoted by nb (no binding). [b] Rejante (1992). [c] Rejante et al. (1991). [d] Ramesh et al. (1987). [e] De Marco et al. (1987). [f] Petros et al. (1989). [g] Hochschwender et al. (1983). [h] Thewes et al. (1990).

Raphson energy minimization that included bond, angle, dihedral, improper, van der Waals, and electrostatic energy terms. A distance-dependent dielectric constant with a nonbonding cutoff of 8 Å was applied. After minimization, the ligand 6-AHA was docked manually by placing it at a position close to the putative K2 lysine binding site while allowing the distance between the Trp^{62} and Trp^{72} ring C7 atoms and the closest ligand carbon atoms to remain at ≥7 Å. Following docking, an adopted-basis Newton Raphson energy minimization was carried out. Calculations were restricted to the side chains of Tyr^{36}, Asp^{55}, Arg^{56}, Glu^{57}, Trp^{62}, Phe^{64}, Arg^{71}, Trp^{72}, Leu^{74}, and 6-AHA. In addition, 15 ligand−kringle distance constraints, which account for the intermolecular NOESY connectivities, and 8 intra-kringle binding site NOE constraints were introduced. Minimizations were repeated five times while decreasing stepwise the contribution of the NOE constraints to zero. In order to optimize the model, conformational space was sampled by runs of molecular dynamics at various temperatures involving the same residues, while the remainder of the K2 structure was frozen in a rigid structure that corresponds to the crystallographic K4 conformation. The ligand-complexed binding site was allowed to accommodate by heating to 310 K (NOE constraints switched off) and thereafter cooling to ~6 K in 620 steps of 10^{-3} ps under Overhauser distance constraints enforcement while maintaining rigid the rest of the molecule. Each temperature change was followed by a 1 ps dynamic equilibration step. After annealing, a final energy minimization was carried out without the NOE constraints.

RESULTS AND DISCUSSION

Expression of r-K1. Approximately 22% of the isolated r-K1 was found in the cytosolic cell fraction, while ~78% of the r-K1 was expressed in the form of inclusion bodies and could be obtained, after refolding, from the insoluble cell debris fraction. Ion exchange chromatography on a Mono-Q column turned out to be efficient for removal of residual 6-AHA bound to the r-K1 domain following the affinity chromatography on lysine−BioGel. The N-terminal sequence analysis indicated the expected sequence M^{77}-K-V-Y-L, confirming the K77M mutation originating from the translation start codon. Molecular mass determination yielded a peak at 10 166 Da, in good agreement with the calculated mass of 10 167 Da. The yield of r-K1 after purification amounted to ~0.9 mg/g of wet cell paste. Disulfide bonds were verified by sequence analysis of proteolytic r-K1 fragments generated by clostripain digestion. A functional lysine binding site, exploited for purification of the domain, affords an additional indication of native folding. ^{1}H-NMR spectra show high-field-shifted Leu^{46} δ-methyl resonances at −1.04 and 0.34 ppm (pH 7.2), as observed in proteolytically derived native HPg K1 (Rejante & Llinás, 1994b), another marker of proper folding. At a concentration of ~0.5 mM and pH 7.2, r-K1 aggregates. Solubility was markedly improved by elastolytic removal of the N-terminal peptide segment M^{77}-K-V.

Expression of r-K2. The recombinant module expressed as the E161T/C162S/EEE[K2/C169S]TT sequence is obtained in yields of ~0.2 mg/g of wet cell pellet (Marti et al., 1994). In order to enhance the expression, a Cys^{169} → Gly mutation was introduced; Gly^{169} is conserved in the sequence of the homologous HPg kringles. In addition, the extra-kringle N- and C-terminal tails of the expressed K2 fragment were each shortened by one amino acid. Expression of r-K2 in the form C162T/E163S/EE[K2/C169G]T improved the yield ~ 6-fold. After FXa cleavage, N-terminal sequence analysis revealed the sequence T^{162}-S^{163}-E-E-X-M-H-G^{169}-S-G, confirming removal of the hexahistidine tail and a correct translation of the N-terminal mutations (C162T, E163S, and C169G). The molecular mass determination yielded the expected mass of 9631 Da. Proper Cys-Cys pairing was verified previously (Marti et al., 1994). r-K2mut was expressed in the form C162T/E163S/EE[K2/C169G/R220G/E221D]T. Mutations C169G, R220G, and E221D were verified by amino acid analysis and electrospray mass spectrometry. Binding of r-K2 and r-K2mut to lysine−BioGel and ^{1}H-NMR spectroscopic criteria confirmed the obtention of properly folded kringles (Söhndel et al., 1996).

^{1}H-NMR Aromatic Spectrum of K2. Sequence alignment of the HPg K2 against the HPg K1, K4, and K5, all homologous lysine-binding domains, reveals pairwise conservancy of 37−39 residues (Figure 1). In K2 and K4, positions[2] 62, 64, and 72 are occupied by Trp, Phe, and Trp residues, respectively, whose exposed aromatic side chains

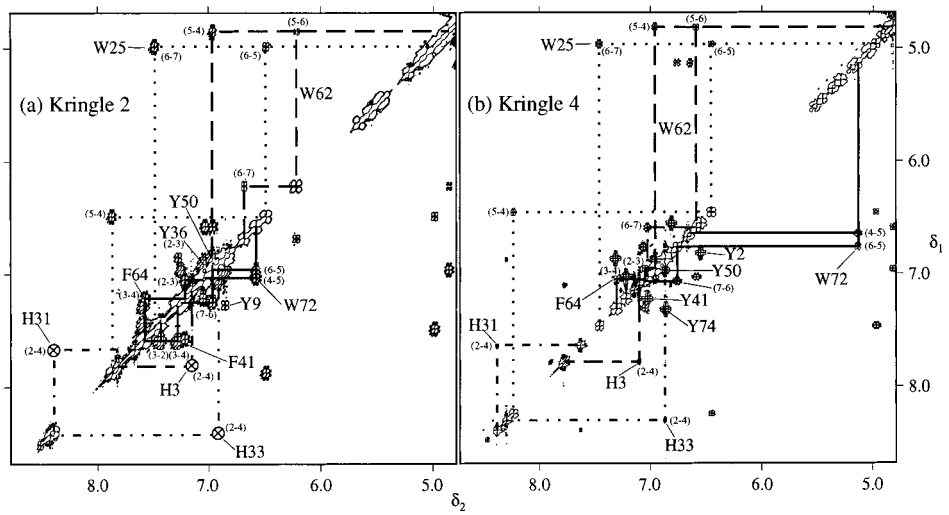

FIGURE 2: Comparison of the aromatic ^{1}H-NMR 2D COSY spectra of HPg r-K2 (a) and proteolytically derived HPg K4 (b). Connectivities are differentiated by various continuous and discontinuous traces. Weak cross-peaks, visible at lower contour plots, are indicated by ⊗. Numbers in parentheses identify the connected proton pair (the matrix convention is used, row proton-column proton). Cross-peaks arising from Tyr^9 ring protons in the K4 spectrum (b) are not observed at the selected contour level. Experimental conditions were as follows: ~0.9 mM kringle samples dissolved in ^2H_2O at pH* 7.2 and 37 °C.

generate the hydrophobic platform that lines the lysine binding site in K4 (Ramesh et al., 1987; Atkinson & Williams, 1990; Wu et al., 1991; Cox et al., 1994). Aromatic ^{1}H-NMR COSY spectra of r-K2 and K4 are displayed in Figure 2. From previous studies (De Marco et al., 1985; Thewes et al., 1990; Rejante & Llinás, 1994b), it has been established that Trp^{25} H6 and Trp^{62} H5 indole resonances of K1, K4, and K5 appear distinctly high-field-shifted between 4.8 and 5.4 ppm. Corresponding signals of r-K2 exhibit a similar pattern (4.94 and 4.81 ppm, Figure 2a). In the case of Trp^{72}, while the H5 resonance is observed at 5.14 ppm in the K4 spectrum (pH 7.2), the corresponding r-K2 signal appears at 6.53 ppm, i.e. closer to 7.17 ppm, the chemical shift of a "random coil" Trp indole H5, suggesting a lesser degree of aromatic packing for the Trp^{72} ring in r-K2 relative to the homologous K4. The complete assignment of the Trp side chain ring protons was confirmed by NOESY and TOCSY ^{1}H-NMR experiments performed on samples dissolved in ^1H_2O. NOESY connectivities between Trp indole ring N3H and C7H/C2H resonances led to an unambiguous identification of all aromatic signals. The low-field spectra of r-K2 and K4 are also remarkably similar in the shift of the Phe^{64}, His^3, His^{31}, and His^{33} resonances (Figure 2a,b).

K2 contains three Tyr residues in positions 9, 36, and 50. Tyr^9 and Tyr^{50} are conserved in all HPg kringles, which assists in their identification. In HPg K1, K4, and K5, Tyr^{50} H2,6 and H3,5 resonances appear between 6.83 and 6.96 ppm (Petros et al., 1988; Thewes et al., 1990; Rejante & Llinás, 1994b), generating COSY cross-peaks close to the diagonal. Expectedly, in r-K2, the Tyr^{50} ring resonances are found at similar spectral positions (6.81 and 6.93 ppm). The aromatic protons of Tyr^{36} in r-K2 yield resonances appearing at 6.87 and 7.00 ppm. NOESY spectra reveal ring−ring connectivities between Tyr^{36} and the Trp^{62} and Phe^{64} side chains. These findings are an indication of the proximity of Tyr^{36} to the cluster of hydrophobic residues at the lysine binding site, similar to what is the case for Phe^{36} in K1 (Rejante & Llinás, 1994a). As for Tyr^9, it typically yields multiple sets of weak COSY cross-peaks in K1, K4, and K5 (not visible in the spectrum of K4 in Figure 2b), reflecting a partially hindered (slow exchange) location of its side chain (Petros et al., 1988). In contrast, only one Tyr^9 aromatic cross-peak is observed in the COSY spectrum of r-K2, at 6.81/7.23 ppm, suggesting a relatively more mobile Tyr^9 aromatic ring in r-K2.

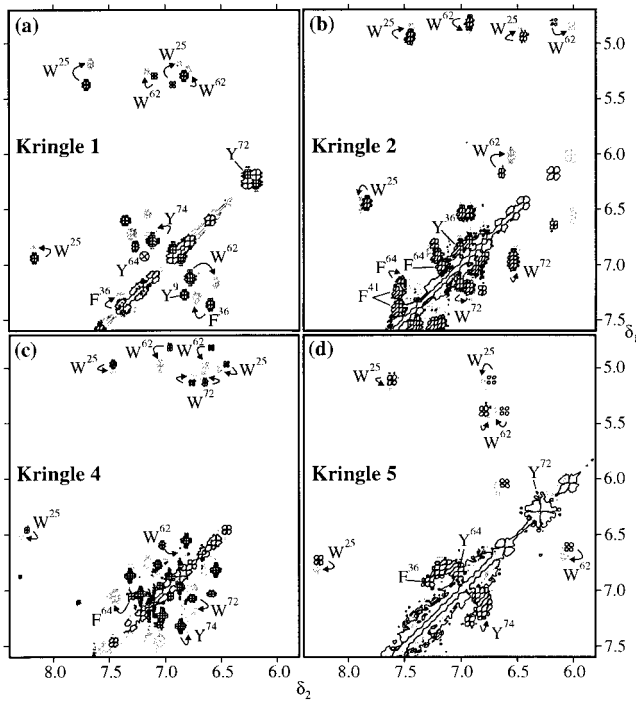

FIGURE 3: ^{1}H-NMR COSY spectra of HPg kringles: response of aromatic resonances to AcLys binding. Kringle spectra in the absence (black) and presence (gray) of ligand are shown superimposed. Ligand excesses of (a) 3-fold, (b) 7-fold, (c) 5-fold, and (d) 70-fold. Ligand-induced cross-peak shifts are denoted by arrows. K4 lacks an aromatic residue in position 36. Tyr^{74}, conserved in K1, K4, and K5, is substituted by a Leu residue in K2. Spectra were obtained from ~0.5 mM kringle samples dissolved in ^2H_2O at pH* 7.2 and 37 °C.

Binding of Linear, Aliphatic Aminocarboxylic Acids to K2. As previously reported (Söhndel et al., 1996), interaction of ligands with kringles results in shifts of resonances, mostly aromatic, stemming from lysine-binding site amino acids perturbed by the complexation (Figure 3). These shifts can be monitored readily and from the ligand titration profiles accurate estimates of the ligand−kringle association constant,

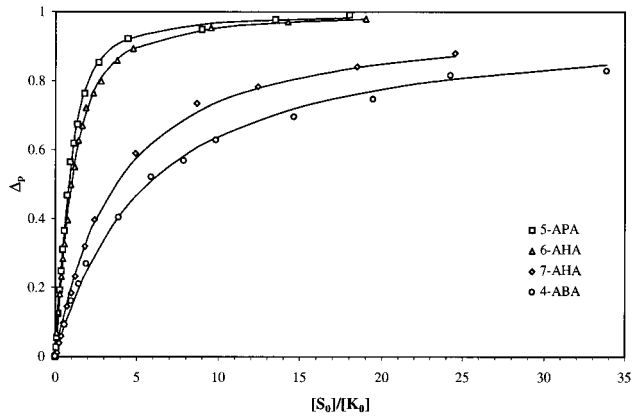

FIGURE 4: K2 ligand titration profiles for the linear aliphatic ω-aminocarboxylic acids 4-ABA, 5-APA, 6-AHA, and 7-AHA. The data depict the fraction of ligand-bound r-K2 (Δ_p) *versus* the total ligand to total kringle ($[S_0]/[K_0]$) concentration ratio. The continuous curves were calculated on the basis of K_a and Δ_p values obtained by iterative nonlinear fitting of the Langmuir adsorption isotherm (eq 2). Data were recorded at pH* 7.2 and 25 °C.

Chart 1: Linear, Aliphatic ω-Aminocarboxylic Acid Ligands

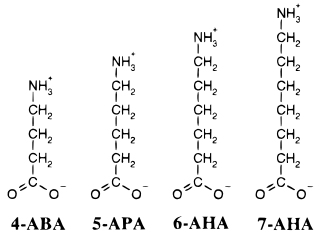

K_a, derived (De Marco et al., 1987). The binding to r-K2 of linear ω-aminocarboxylic acids (Chart 1) with a variable zwitterionic dipole length *l* (4.85 Å < *l* < 8.65 Å) was investigated in order to uncover ligand preferences and test the approximate dimensions of the lysine binding site in r-K2. Figure 4 depicts r-K2 binding profiles for the ligands 4-aminobutyric acid (4-ABA), 5-aminopentanoic acid (5-APA), 6-aminohexanoic acid (6-AHA), and 7-aminoheptanoic acid (7-AHA). 5-APA, with a $COO^- - N^{\delta}H_3^+$ dipole length *l* of ~6.19 Å, exhibits the strongest interaction with r-K2 ($K_a \sim 3.4$ mM^{-1}). 6-AHA ($l \sim 7.33$ Å) binds slightly less firmly ($K_a \sim 2.3$ mM^{-1}). With respect to 5-APA and 6-AHA, both 4-ABA and 7-AHA ($l \sim 4.85$ and 8.65 Å, respectively) are weaker ligands for r-K2 ($K_a \sim 0.22$ and 0.45 mM^{-1}, respectively).

^{1}H-NMR titration experiments of r-K1 with the linear aliphatic ligands yield K_a values of ~5.1 mM^{-1} for 4-ABA, ~44.6 mM^{-1} for 5-APA, ~74.2 mM^{-1} for 6-AHA, and ~13.8 mM^{-1} for 7-AHA. The ^{1}H-NMR titration data are in overall good agreement with results reported by Menhart et al. (1991) on the basis of calorimetric and fluorescence titration experiments. Unlike r-K2, the ligand that exhibits the highest binding affinity for r-K1 is 6-AHA, which is also the preferred ligand for K4 and K5 ($K_a \sim 21$ and 10.6 mM^{-1}, respectively) (Thewes et al., 1990; Rejante et al., 1991; McCance et al., 1994). Although a substantial interaction of 5-APA with both r-K1 and K4 is observed ($K_a \sim 44.6$ and 16 mM^{-1}, respectively), such is not the case for K5 ($K_a \sim 0.72$ mM^{-1}). The dependency of K_a on the ligand dipole length *l* is illustrated in Figure 5a. It is apparent that K5 exhibits the most stringent dependency on *l*; relative to 6-AHA, the ~1.14 Å shorter 5-APA ligand interacts ~15 times more weakly with K5, whereas in the case of r-K1,

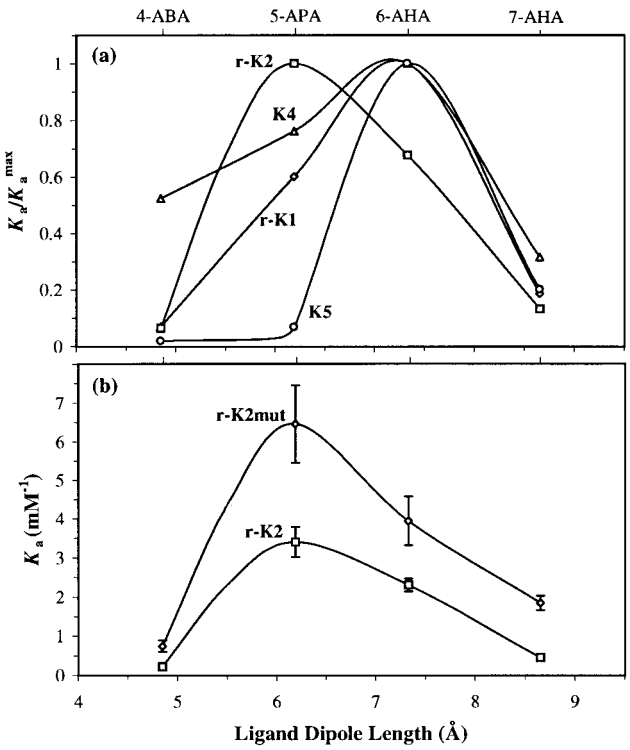

FIGURE 5: Affinities of HPg kringles for linear aliphatic ω-aminocarboxylic acids: dependence on the ligand zwitterionic dipole length *l*. (a) Comparison of r-K1, r-K2, K4, and K5. K_a values are normalized relative to each kringle's highest K_a value (K_a^{max}). (b) Comparison of r-K2 and r-K2mut. The dipole length *l* is defined as the distance between the distal amino nitrogen and carboxylate carbon atoms for the molecules in the extended conformation. The continuous curves are arbitrary interpolations between the experimental data points. Experimental conditions were as described for Figure 4.

r-K2, and K4, the preference for 6-AHA over 5-APA (5-APA over 6-AHA in case of r-K2) is less pronounced. With regard to 4-ABA, K4 exhibits the highest binding affinity among the four lysine-binding kringles ($K_a \sim 11$ mM^{-1}) while K5 and r-K2 show only marginal affinity for this ligand ($K_a \sim 0.2$ mM^{-1}).

Among the investigated kringles, all except r-K2 contain an Asp residue at site 57 which, according to the consensus model, interacts with the cationic end amino group of the ligands (Llinás et al., 1983; Tulinsky et al., 1988b). In K2, Asp^{57} is replaced by Glu^{57}. Also, lysine-binding kringles 1, 4, and 5 fill site 56 with a nonpolar, electrostatically neutral residue, while K2 carries an Arg at this position, so that interference with the Asp^{55}/Glu^{57}-mediated ligand-binding interaction might be expected. To investigate the effect of these substitutions on the K2 ligand-binding selectivity, an r-K2mut was expressed in which Arg^{56} and Glu^{57} were exchanged for Gly and Asp, respectively. Expectedly, the mutant shows an improved ability to bind all of the tested linear ligands (Figure 5b). However, as is the case for r-K2, 5-APA ($K_a \sim 6.5$ mM^{-1}) is the preferred ligand for r-K2mut as well, with 6-AHA showing a slightly weaker binding ($K_a \sim 3.9$ mM^{-1}). Similarly, mimicking the binding properties of "wild-type" r-K2, 6-AHA is preferred over 7-AHA ($K_a \sim 1.8$ mM^{-1}) and the latter over 4-ABA ($K_a \sim 0.74$ mM^{-1}). These results indicate that the Asp^{57} → Glu substitution in K2 affects only the overall efficiency for binding, but not the K2 linear ligand specificity. This goes against conventional wisdom as the Asp side chain, being ~1.2 Å shorter than the corresponding Glu side chain, would be expected

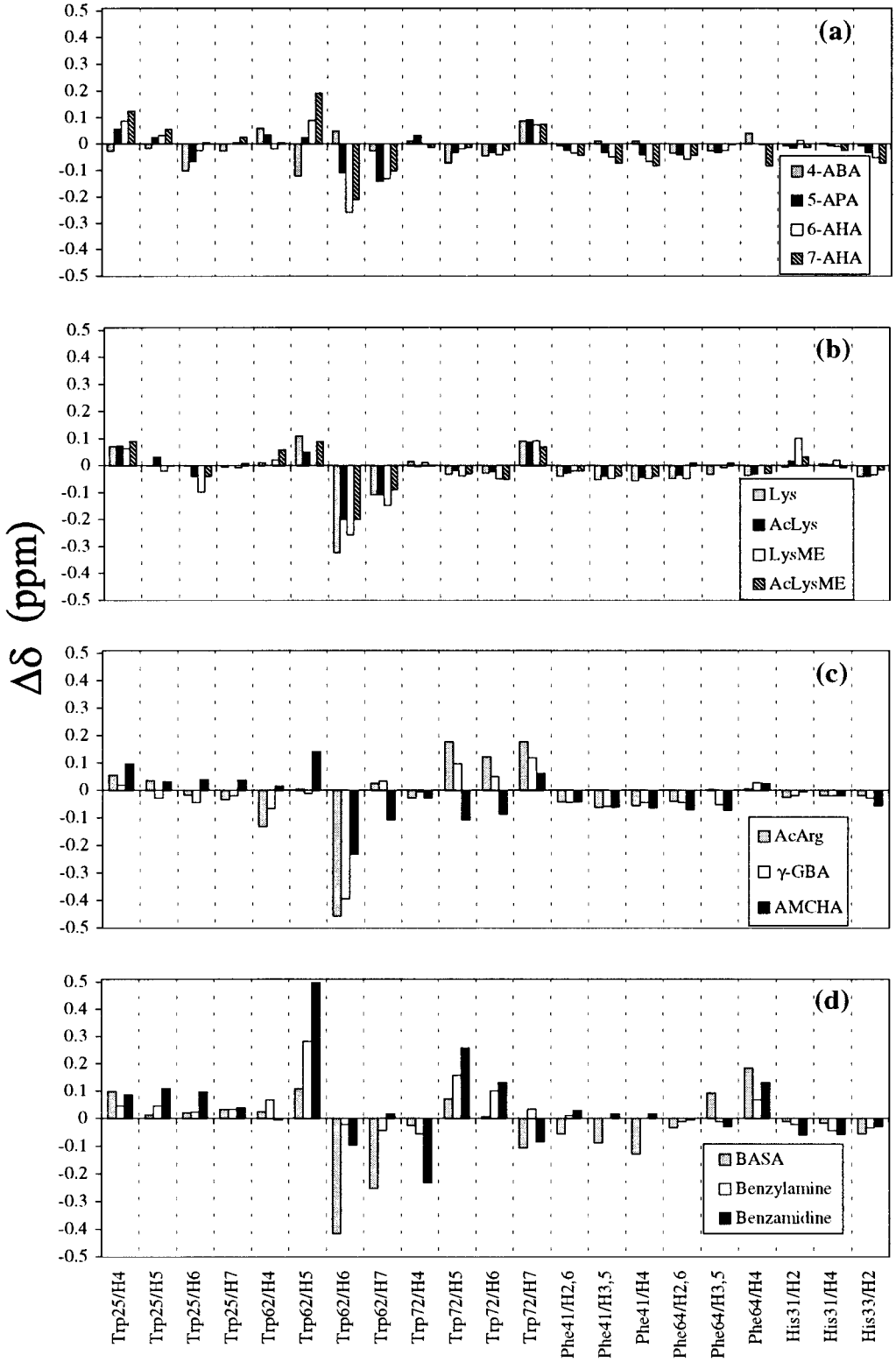

FIGURE 6: Ligand-induced shifts ($\Delta\delta$) of selected r-K2 aromatic ring proton resonances. Shifts caused by linear aliphatic ω-aminocarboxylic acids (a), lysine derivatives (b), AcArg, γ-GBA, and AMCHA (c), and aromatic ligands (d) are illustrated in a bar graph representation. Bars of positive and negative amplitude represent low- and high-field shifts, respectively. Data were extracted from 2D COSY spectra.

to accommodate 6-AHA, a longer ligand, better than 5-APA. Thus, the enhanced binding profile of r-K2mut relative to r-K2 may be interpreted to stem mainly from the $Arg^{56} \rightarrow$ Gly mutation, as the presence of a cationic Arg side chain positioned between Asp^{55} and Glu^{57} can only weaken the net (negative) electrostatic potential at the binding site anionic locus.

Ligand-induced shifts of r-K2 aromatic and His imidazole ring resonances are summarized in Figure 6a. ^{1}H-NMR signals stemming from Trp^{62} H5/H6/H7 are the most affected by the ligand, most noticeable with 5-APA, 6-AHA, and 7-AHA. A distinct ligand-induced perturbation is also observed for the Trp^{25} H4/H6 and Trp^{72} H7 signals. Ring resonances of Phe^{64} and Phe^{41} shift comparably except for the Phe^{64} H4 which is not significantly affected by 5-APA or 6-AHA. As for His^{31} and His^{33}, located in the periphery of the binding site, only the latter's imidazole H2 signal undergoes definite ligand-induced shifts.

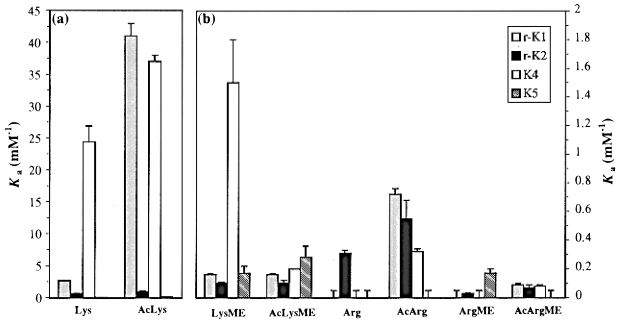

FIGURE 7: Bar graph summary of equilibrium association constants for lysine and arginine derivatives interacting with HPg kringles. Weak ligand associations (K_a < 0.03 mM^{-1}) are denoted by a half-error bar (T). As indicated, ordinate scales for panels a and b differ. Experimental conditions were as described for Figure 4.

Binding of Lysine and Derivatives to K2. Among L-lysine (Lys) and its N$^{\alpha}$/C′-blocked derivatives (Chart 2), *N*$^{\alpha}$-acetyl-L-lysine (AcLys) is the one ligand which shows the most stable interaction with the r-K2 domain ($K_a \sim 0.96$ mM^{-1}). It is interesting that despite the relatively weak binding when compared against r-K1 and K4 ($K_a \sim 41$ and 37 mM^{-1}, respectively) (De Marco et al., 1987; Rejante, 1992), the r-K2 affinity for an N$^{\alpha}$-blocked L-lysine ligand is sufficient to retain it on lysine−BioGel, the matrix used for its affinity chromatographic purification. Also noteworthy is the fact that K5, which relative to r-K2 shows an affinity for 6-AHA ∼4 times higher, exhibits an ∼5-fold weaker interaction with AcLys ($K_a \sim 0.18$ mM^{-1}). Consistent with these results, binding of K5 to lysine-substituted chromatographic gel matrices, either as a single domain or in covalent association with the protease domain (mini-plasminogen), has not been detected (Sottrup-Jensen et al., 1978; Novokhatny & Kudinov, 1984). Unblocking of the ligand α-amino group, like on going from AcLys to Lys, effects a slight decrease in the binding affinity with respect to r-K2 ($K_a \sim 0.68$ mM^{-1}). A similar (∼1.5-fold) decrease in the binding affinity was observed on going from AcLys to Lys for the K4 and K5 domains; $K_a \sim 24.4$ and ∼0.1 mM^{-1}, respectively (Ramesh et al., 1987; Thewes et al., 1990). In the case of r-K1, its lysine binding affinity depends even more markedly on the occurrence of an unblocked α-amino group; an ∼15-fold drop in affinity has been determined on going from AcLys ($K_a \sim 41$ mM^{-1}) to Lys ($K_a \sim 2.7$ mM^{-1}) (Rejante, 1992).

On the basis of what is known for other kringles, lysine containing an esterified C′ carboxyl group (LysME) was expected to exhibit only weak binding to r-K2 ($K_a \sim 0.1$ mM^{-1}). Additional blocking of the α-amino group (AcLysME) has no significant effect on the binding interaction, as previously observed for r-K1 which exhibits a K_a of ∼ 0.16 mM^{-1} for both LysME and AcLysME (Rejante, 1992). K4 however favors LysME ($K_a \sim 1.5$ mM^{-1}) relative to AcLysME ($K_a \sim 0.2$ mM^{-1}) which suggests steric hindrance effects (Petros et al., 1989). Interestingly, among the lysine derivatives, K5 shows a preference for AcLysME ($K_a \sim 0.28$ mM^{-1}).

The diagram in Figure 7 summarizes K_a data for the lysine-type ligands. It is apparent that among the kringles the differences in K_a for AcLysME, a ligand which mimics an internal lysine residue within a polypeptide chain, are much less pronounced than they are for Lys, AcLys, or LysME. These results suggest that all the lysine-binding kringles of HPg are potentially capable of interacting with intrachain lysine residues, whereas the strong preference for binding

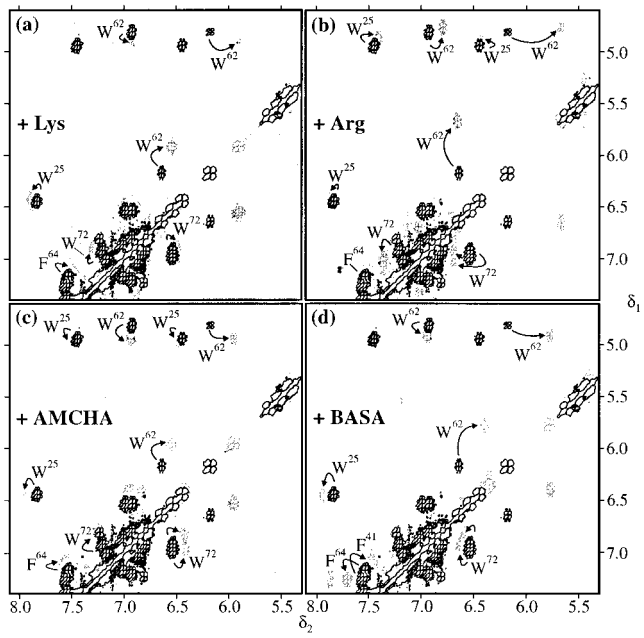

FIGURE 8: Aromatic ^{1}H-NMR COSY spectra of HPg r-K2 in response to the ligands Lys (a), Arg (b), AMCHA (c), and BASA (d). Spectra in the absence (black) and presence (gray) of effector have been superimposed. Ligand excesses of (a) 13-fold, (b) 50-fold, (c) 16-fold, and (d) 22-fold. Ligand-induced cross-peak shifts are denoted by arrows. Experimental conditions were as described for Figure 3.

Chart 2: Lysine Ligands

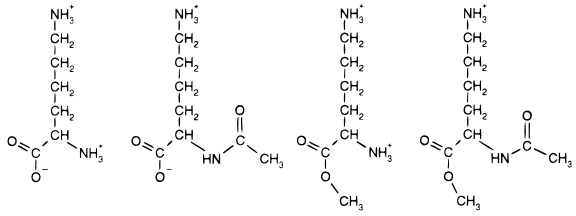

C-terminal lysine, as probed by the AcLys ligand, would seem to be a property of mainly K1 and K4, the latter also showing a relatively favored affinity for LysME, which models an N-terminal Lys locus.

It has been verified by NMR and X-ray crystallographic studies on K1 complexed to 6-AHA that the ligand hydrocarbon backbone maintains close van der Waals contacts with the side chains of residues Trp^{62}, Tyr^{64}, and Tyr^{72} and, to a lesser extent, with those of Phe^{36} and Tyr^{74} (Rejante & Llinás, 1994a; Mathews et al., 1996). In K4, residues Trp^{62}, Phe^{64}, Trp^{72}, and possibly Tyr^{74} have been shown to variously contribute to hydrophobic interactions with the ligand (Rejante et al., 1991; Wu et al., 1991). The perturbations of aromatic spectra of r-K1, r-K2, K4, and K5 by AcLys are clearly visible from COSY experiments (Figure 3). Superposition of r-K2 spectra in the absence and presence of the ligand reveals distinct shifts of Trp^{25}, Trp^{62}, and Trp^{72} ring ^{1}H resonances (Figure 3b). Small ligand-induced shifts are also observed for the aromatic signals of Tyr^{36}, Phe^{41}, and Phe^{64}. In the case of r-K1, K4, and K5, ligand addition rather uniformly affects residues in corresponding positions (Figure 3a,c,d). Qualitatively, the Lys-induced aromatic shifts for r-K2 (Figure 8a) are similar to those resulting from complexation by AcLys (Figure 3b), confirming binding interactions with essentially the same constellation of side chains at the binding site.

Chart 3: Arginine-Related Ligands

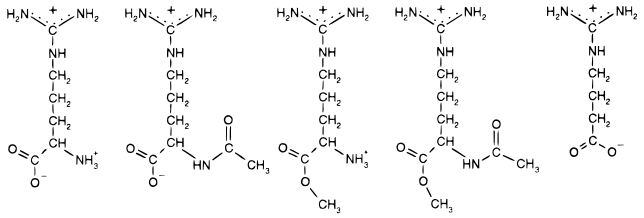

Chart 4: Cyclic Ligands

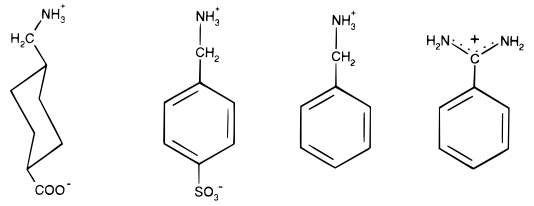

The diagram in Figure 6b summarizes the chemical shift response of selected aromatic and His imidazole ring resonances of r-K2 upon binding Lys derivatives. Most of the perturbations of Trp and Phe ring resonances are comparable in magnitude for the various effectors. Trp^{25} H4, Trp^{62} H5/H6/H7, and Trp^{72} H7 signals are distinctly affected by the Lys ligands. For most resonances, the direction of the induced chemical shifts is consistent with the spectral perturbations resulting from 5-APA, 6-AHA, or 7-AHA binding, indicative of similar interactions of the linear aliphatic and Lys-type ligands with the r-K2 binding site.

Binding of Arginine and Derivatives to K2. Although HPg kringles exhibit overall rather weak interaction with L-arginine (Arg) derivatives, conceivably, Arg side chains exposed by clotted fibrin could compete *in vivo* with Lys sites for binding HPg via the kringles' binding sites. K1 and K4 measurably bind N^{α}-acetyl-L-arginine (AcArg) ($K_a \sim 0.72$ and 0.32 mM^{-1}, respectively) and N^{α}-acetyl-L-arginine methyl ester (AcArgME) ($K_a \sim 0.09$ and 0.08 mM^{-1}, respectively), whereas specific interactions with Arg or L-arginine methyl ester (ArgME) have been found to be undetectable by ^{1}H-NMR ($K_a < 0.03$ mM^{-1}) (Chart 3) (Rejante et al., 1991; Rejante, 1992). Surprisingly, among the Arg ligands, the K5 binding site interacts only with ArgME ($K_a \sim 0.17$ mM^{-1}) (Thewes et al., 1990). Comparative K_a data for the Arg ligands are summarized in Figure 7b. Among the Arg ligands, AcArg is the one which binds the most to r-K2 ($K_a \sim 0.55$ mM^{-1}). As illustrated in Figures 6c and 8b, Arg-type ligands cause relatively extensive shifts on the Trp^{62} H4 (approximately −0.13 ppm), Trp^{62} H6 (approximately −0.46 ppm), and Trp^{72} H5/H6/H7 (∼0.15 ppm) resonances. With a K_a of ∼0.31 mM^{-1}, the affinity of r-K2 for Arg is ∼1.8 times weaker than that for AcArg. This is similar to the case for the lysine derivatives discussed above, showing an ∼1.4-fold lower K_a for Lys relative to AcLys. Thus, it is suggested that blockage of the positive electrostatic charge at the ligand N^{α}-amino group strengthens the Coulombic interaction between kringle basic residues and the ligand carboxylate group. Blockage of the carboxylate group in AcArg and Arg results in an ∼8−10-fold decrease in the binding affinity ($K_a \sim 0.07$ and 0.03 mM^{-1}, respectively). However, in contrast to the case for LysME and AcLysME, which yield identical K_a's for r-K2, the relative binding affinities of the Arg derivatives with blocked carboxylate group are consistent with an extent of dependence on the N^{α}-amino group electrostatic charge as discussed above so that neutralizing the electrostatic charge on the α-amino group raises the efficiency for ligand binding.

The binding affinity of r-K2 for γ-guanidinobutyric acid (γ-GBA) was also investigated; in arginine, the extended chain distance between the caboxylate and the guanidino group is ∼7.9 Å, while in γ-GBA, the corresponding distance between the two polar groups amounts to ∼6.84 Å. Our experiments reveal that relative to AcArg ($K_a \sim 0.55$ mM^{-1}) γ-GBA is a weaker ligand for r-K2 ($K_a \sim 0.28$ mM^{-1}). In contrast, r-K1 and K4 definitely favor γ-GBA ($K_a \sim 2.8$ and 2.6 mM^{-1}, respectively) over AcArg ($K_a \sim 0.72$ and 0.32 mM^{-1}, respectively), while K5, which shows negligible interaction with AcArg, binds γ-GBA with an affinity comparable to that of r-K2 ($K_a \sim 0.37$ mM^{-1}). The clear preference of r-K1, K4, and K5 for γ-GBA vis-à-vis AcArg is probably not just a manifestation of the shorter chain length of γ-GBA but also of the absence in the latter of an α-amino group, which eliminates potential electrostatic and/or steric hindrance effects. On these grounds, we would not expect to find this same ligand to yield for r-K2 an effect opposing the trend suggested by the K1, K4, and K5 homologs.

AMCHA Binding to K2. The antifibrinolytic drug *trans*-(aminomethyl)cyclohexanecarboxylic acid (AMCHA) which is known to interact tightly with Lys-binding kringles was tested for its affinity for r-K2. Among the investigated aliphatic zwitterions, AMCHA also turns out to be the strongest ligand for r-K2 ($K_a \sim 7.3$ mM^{-1}). In its chair conformation (Chart 4), AMCHA yields an *l* of ∼6.16 Å for the amino/carboxylate dipole. In comparison to 5-APA, a linear ligand with a comparable dipole length ($l \sim 6.19$ Å), the ∼2-fold increase in binding affinity for AMCHA could stem from the more extended surface of the nonplanar cyclohexane ring for lipophilic interaction with aromatic residues at the kringles' lysine binding site. This is in line with the marked rise in K_a on going from 5-APA to AMCHA in r-K1, K4, and K5 which exhibit K_a values of >300, ∼159, and ∼44.2 mM^{-1}, respectively, for the cyclic ligand.

Figure 8c illustrates the shifts of aromatic COSY cross-peaks induced by AMCHA on r-K2. In particular, the resonances of Trp^{25} H4, Trp^{62} H5/H6/H7, and Trp^{72} H5/H6 are distinctly affected by ligand presence and the shift in the same direction as observed for the lysine derivatives and the linear aliphatic ligands 5-APA, 6-AHA, and 7-AHA (Figure 6a−c). The perturbation of the same set of aromatic signals in response to AMCHA confirms that it is the canonical lysine binding site that mediates the interaction of K2 with the ligand.

As reported (Rejante et al., 1991; Rejante, 1992), ^{1}H-NMR spectra of K1 and K4 in the presence of AMCHA exhibit high-field-shifted signals from the bound ligand, reflecting anisotropic ring-current effects caused by contacting aromatic groups from residues at the binding site. Such shifted ligand resonances are not observed at 500 MHz for the r-K2−AMCHA complex, suggesting somewhat faster on−off ligand exchange kinetics in agreement with the weaker affinity of AMCHA for r-K2 relative to that for the homologous kringles.

Interaction of Aromatic Ligands with K2. The binding of the aromatic ligands *p*-benzylaminesulfonic acid (BASA), benzylamine, and benzamidine (Chart 4) to r-K2 was also investigated. BASA contains amino and sulfonate groups

para to each other, with an *l* of ~6.64 Å across the benzyl group. In comparison to AMCHA ($K_a \sim 7.3$ mM^{-1}), BASA shows weak binding to r-K2 ($K_a \sim 4$ mM^{-1}). Besides a longer dipole distance *l*, the rigid planar aromatic ring of BASA is likely to be less suitable for establishing as intimate a contact with the binding site hydrophobic residues as AMCHA does. However, reflecting its aromatic character, BASA most markedly shifts the resonances of Trp[25] H4, Trp[62] H5/H6/H7, and Trp[72] H5/H7 (Figure 8d). Furthermore, the Phe[41] H3,5/H4 and Phe[64] H3,5/H4 signals, which show only moderate shifts in the presence of aliphatic ligands, are affected extensively by BASA (Figure 6d). In contrast, both benzylamine and benzamidine, the latter's amidino group carrying a positive electric charge, exhibit weak interactions with r-K2 ($K_a \sim 0.04$ and 0.03 mM^{-1}, respectively). This underscores the requirement of a highly polar, anionic center, such as that afforded by the sulfonate group in BASA, for stable ligand binding; in turn, it confirms the marginal, although by no means negligible, contribution of the ligand benzenoid ring to the intermolecular interaction.

The binding affinities of K1 and K4 for BASA are ~4 and ~2 times weaker, respectively, than that for AMCHA. As discussed above for benzylamine and benzamidine binding to r-K2, the absence of an anionic group in the ligand leads to a marked reduction in ligand-binding affinity. However, the aromatic ligands behave differently in the case of K5, whose interaction with BASA is ~20 times weaker when compared against that of AMCHA. Interestingly, removal of the negative charge from the ligand increases the latter's binding affinity for K5, as exemplified by benzylamine and benzamidine.

^{1}H-NMR-derived ligand association constants for r-K2 and for the homologous lysine-binding HPg kringles are listed in Table 1.

Molecular Model of the K2 Lysine Binding Site. Structures of the K2 lysine binding site complexed to 6-AHA were calculated starting from the crystallographic structure of ligand-free K4 (Mulichak et al., 1991), as this homolog exhibits the highest binding site residue conservancy with K2 (Figure 1). After mutations R32A, Q34G, K35Y*, A56R, D57E, and Y74L were introduced, energy minimization and molecular dynamics calculations were performed. The force field incorporated (i) 8 intramolecular NOE distance constraints between aromatic protons at the binding site and (ii) 15 intermolecular NOE distance constraints connecting ligand α-, *β*-, and *γ*-protons to side chain aromatic protons at the binding site (Figure 9 and Table 2). In the final round of energy minimization, the NOE distance constraints were relaxed. The resulting structures could be grouped into two subsets which differ mainly in the spatial orientation of the Arg[56] and Glu[57] side chains (Figure 10A,B). In HPg K1 and K4, the location of the Asp[57] carboxylate group is stabilized by a hydrogen bond to the hydroxyl group of Tyr[74] (Wu et al., 1991; Mathews et al., 1996). In K2, Tyr[74] is substituted by Leu[74], which exposes a hydrophobic side chain. As a consequence, the spatial orientation of the Glu[57] side chain is somewhat less restricted, which has the potential to affect the ability of K2 to establish a stable interaction with the ligand. In structure A, the anionic side chain groups of Arg[56] and Glu[57] are poised to form a salt bridge which results in ~90 and ~75° angles between the Glu[57] $C^\gamma-C^\delta$ bond and the longitudinal and latitudinal axes of the binding site as configured by the side chain indole rings of Trp[62] and Trp[72]. Therefore, when compared against

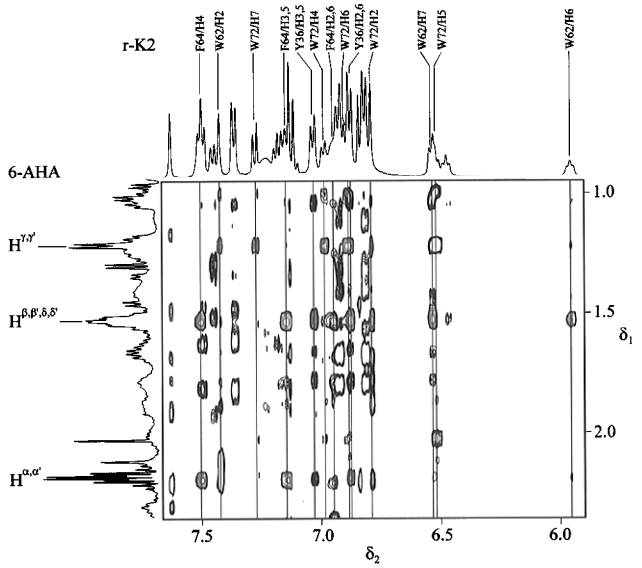

FIGURE 9: ^{1}H-NMR NOESY spectrum of r-K2 complexed to 6-AHA. Cross-peaks originating from ligand H^α, H^β, and H^γ protons in contact with aromatic residues of the kringle lysine binding site are denoted in red. The highlighted cross-peak volumes were measured and used to estimate intermolecular distances. Corresponding segments of the 1D spectra are shown. Experimental conditions were as follows: ~1.9 mM kringle solution ([r-K2]/[6-AHA] ~ 1/7) in ^2H_2O at pH* 7.2 and 37 °C; mixing time of 300 ms.

Table 2: Lysine Binding Site of the r-K2 Complexed to 6-AHA and the Proton Overhauser Distance Constraints

proton pairs		
1	2	distance (Å)[a]
Trp[62]/H5	Phe[64]/H3	3.0
Trp[62]/H6	Trp[72]/H6	3.1
Trp[62]/H6	Tyr[36]/H3,5	3.3
Trp[62]/H6	Phe[64]/H3,5	2.9
Trp[62]/H6	Phe[64]/H4	2.9
Phe[64]/H3,5	Tyr[36]/H3,5	3.5
Phe[64]/H4	Tyr[36]/H2,6	2.9
Phe[64]/H4	Tyr[36]/H3,5	2.7
$C^\gamma H_2$	Trp[62]/H2	3.2
$C^\gamma H_2$	Trp[72]/H2	3.7
$C^\gamma H_2$	Trp[72]/H4	3.3
$C^\gamma H_2$	Trp[72]/H6	2.9
$C^\gamma H_2$	Trp[72]/H7	3.6
$C^\beta H_2$	Tyr[36]/H2,6	2.9
$C^\beta H_2$	Tyr[36]/H3,5	3.3
$C^\beta H_2$	Trp[62]/H6	3.2
$C^\beta H_2$	Trp[62]/H7	2.7
$C^\beta H_2$	Phe[64]/H3,5	2.7
$C^\beta H_2$	Phe[64]/H4	3.1
$C^\beta H_2$	Trp[72]/H2	2.7
$C^\alpha H_2$	Tyr[36]/H2,6	3.3
$C^\alpha H_2$	Phe[64]/H3,5	3.1
$C^\alpha H_2$	Phe[64]/H4	3.0

[a] Cross-peak volumes were obtained from a NOESY experiment at 37 °C with a τ_{mix} of 125 ms. Distances were calculated by reference to intra ring Trp indole cross-peaks. C^α, C^β, and C^γ denote carbon atoms of the ligand.

K1 and K4, the residue 57 anionic locus results in being more distant from the binding site lipophilic surface contributed mainly by the Trp[62], Phe[64], and Trp[72] aromatic groups. Thus, the ligand amino group, which interacts with both Asp[55] and Glu[57] (Motta et al., 1987; Ramesh et al., 1987; Wu et al., 1991; Mathews et al., 1996), positions itself further removed from the longitudinal axis of the binding site. This would preclude intimate hydrophobic contact of the ligand

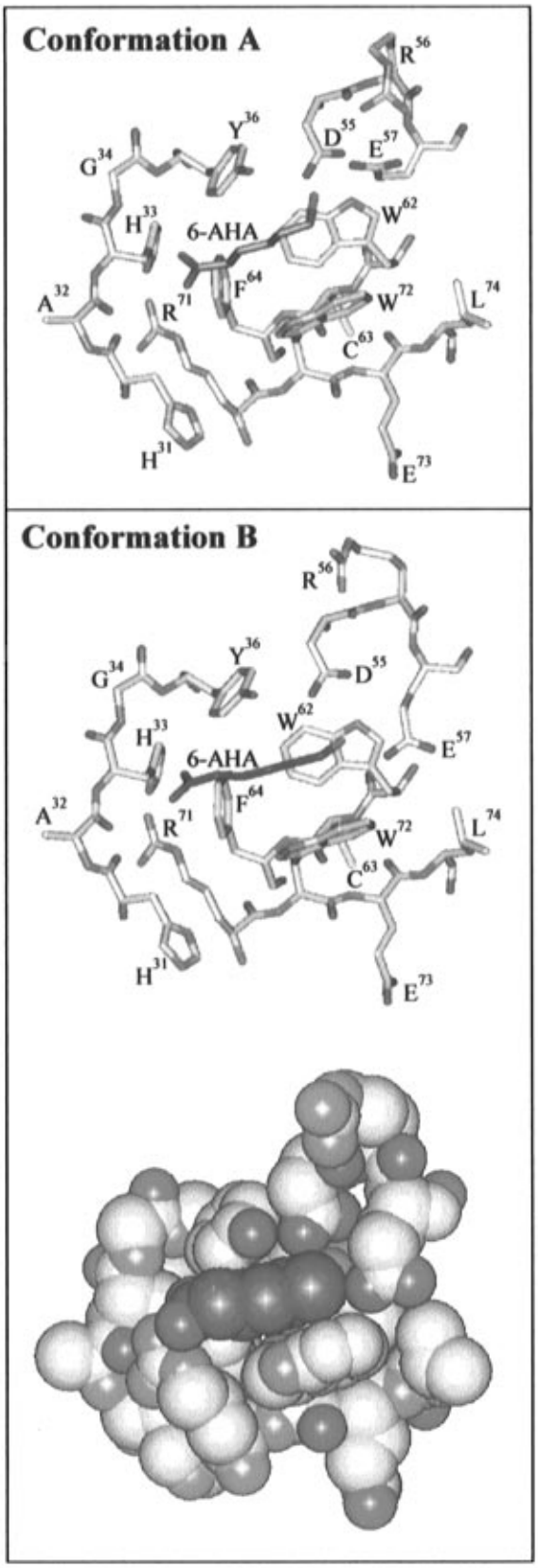

FIGURE 10: Molecular model of the K2 lysine binding site complexed to 6-AHA. Included are the K2 segments His^{31}−Tyr^{36}, Asp^{55}−Glu^{57}, Trp^{62}−Phe^{64}, and Arg^{71}−Leu^{74}. The ligand molecule is colored magenta. Polar group N and O atoms are denoted in blue and red, respectively. Computed conformations A and B differ mainly in the spatial orientation of the side chains of Arg^{56} and Glu^{57}, which pair through ionic interaction in conformation A but not in conformation B, also shown in a space filling (effective van der Waals radii) representation (bottom). The model was derived from the NOE distance constraints (Table 2) starting from the crystallographic structure of K4 (Mulichak et al., 1991).

δ- and ϵ-methylene groups with the Trp^{62} and Trp^{72} side chain rings. In structure B, the Glu^{57} C$^{\gamma}$−C$^{\delta}$ bond remains perpendicular to the longitudinal axis of the binding site. However, the angle with the latitudinal axis of the subjacent binding site groove is approximately −45°, in contrast to ∼75° for structure A. The δ-carboxylate group of Glu^{57} distances itself from the Trp^{62} C2 and Trp^{72} C6 atoms by ∼4.8 and ∼4.4 Å, respectively, whereas in structure A, these distances are consistently larger, ∼6.4 Å. The closer proximity of the Glu^{57} C$^{\delta}$OO^{-} group to the hydrophobic side chains of Trp^{62} and Trp^{72} in model B leads to a more favorable contact between the ligand hydrocarbon backbone and the aromatic rings; the distances between the ligand C$^{\epsilon}$ and Trp^{62} N3 and Trp^{72} C7 are ∼6.0 and ∼4.2 Å, respectively, for structure A and ∼4.2 and ∼3.7 Å, respectively, for structure B.

In both models, the spatial position of the carboxylate group of Asp^{55} is stabilized via hydrogen bonding to the ring NH of Trp^{62} (Figure 10A,B). The carboxylate group of the ligand maintains an ionic interaction with the side chain of Arg^{71} which, in turn, is thought to generate H bonding to the Ala^{32} carbonyl group. Also, the location of the Tyr^{36} side chain is constrained by an H bond involving its side chain hydroxyl and the carboxylate group of Asp^{55}. The distance between the guanidino group of Arg^{71} and the δ-carboxylate group of Glu^{57} which roughly defines the length of the binding site amounts to ∼13.7 and ∼13.3 Å for structures A and B, respectively. Similar values of ∼13.1 (A) and ∼13.7 Å (B) are obtained for the distance between the Arg^{71} guanidino group and the Glu^{57} C$^{\gamma}$. These model-based findings agree with the observation that, although relative to r-K2, r-K2mut (containing mutations R56G and E57D) displays stronger interactions with each of the investigated linear aliphatic ligands, the dependency of the K_a on the ligand chain length is similar to that observed for r-K2 (Figure 5b). In particular, structure A suggests that the E57D mutation, which shortens the site 57 acidic side chain by a methylene group unit, places the carboxylate group closer to the longitudinal axis of the binding site, thus leading to a potentially more facile hydrophobic contact of the bound ligand hydrocarbon backbone with the exposed binding site aromatic groups.

CONCLUSIONS

The overall characteristics of the r-K2 ^{1}H-NMR spectrum, the most noteworthy being the presence of the high-field-shifted Leu^{46} methyl signals (Söhndel et al., 1996), afford powerful evidence for correct folding of the expressed module. Furthermore, the similar appearance of wide sections of the r-K2 and K4 aromatic spectra (Figure 2) reinforces a close structural relatedness between the two domains, most significant in the location of residues at the putative binding site. Thus, the side chain ring resonances of Trp^{25}, Trp^{62}, Phe^{64}, Tyr^{50}, His^{3}, His^{31}, and His^{33} exhibit chemical shifts which agree remarkably well between the two homologs. This concurs, as shown in this study, with r-K2 bearing a functional lysine binding site with affinity for zwitterionic/cationic ligands such as simple linear aliphatic molecules, including lysine and arginine derivatives, as well as cyclic aliphatic and aromatic analogs.

However, in contrast to K1, K4, and K5 which, among the linear aliphatic ligands, show a preference for 6-AHA, the K2 domain exhibits a higher affinity for 5-APA. As

demonstrated by r-K2mut, which contains Gly and Asp residues at loci 56 and 57, the preference for the shorter ligand is apparently not a direct consequence of the $Asp^{57} \rightarrow Glu$ substitution in wild-type K2.

On the basis of the relatively weak binding affinity of r-K2 for linear ligands and its preference for 5-APA, structural as well as dynamical differences in the lysine binding site of K2 relative to HPg K1, K4, and K5 are suggested. NOESY data for r-K2 in the presence of 6-AHA indicate that the aromatic side chains which contact the ligand are in positions equivalent to those identified in K1 and K4 binding sites. However, the lack of a basic residue (Arg and Lys in K1 and K4, respectively) at site 35 and the absence of a Tyr at site 74 are suggested to result in a less favorable constellation of side chains for ligand binding. It should be recalled that, besides contributing lipophilic character to the binding sites of K1, K4, and K5, Tyr^{74} also regulates the orientation of the binding site Asp^{57} side chain. In particular, the ability of Arg^{56} and Glu^{57} to ion-pair in K2 would further lower its ligand-binding efficiency. Assuming a possible coexistence of conformers A and B (Figure 10), the lesser hydrophobic interaction with the ligand in structure A would lead to a reduced K_a for K2.

A main function of kringle domains in proteins is the mediation of inter- and intramolecular interactions. In HPg, kringles are thought to be responsible for substrate recognition (fibrin, cell surface receptors, tissue matrix proteins, etc.) and to play a regulatory role in the activation of HPg. Relative to K2 or K5, K1 and K4 show significantly higher affinities for AcLys (Table 1), a ligand which models a C-terminal lysine. In contrast, the affinity for AcLysME, which models an intra-peptide chain lysine, is very similar for K1, K2, K4 and K5. Also in the cases of AcArg and AcArgME, K1 and K4 exhibit binding properties similar to those of r-K2. These results are significant in that they suggest that, other factors being equal, in intact HPg the K2 module might be capable of interacting with intra-peptide chain lysines and/or arginines on the same footing as K1, K4, or K5 do. Thus, K2 is likely to be an equal partner in substrate recognition as well as in the regulation of the activation of HPg. Additional investigations on multidomain fragments of HPg should help clarify the relative extents of functional autonomy of, as well as cooperative interactions among, the HPg kringles. Furthermore, results from this study might be helpful for the design of better fibrinolytic inhibitors that could bind simultaneously to more than one kringle, presumably with higher affinity than the monovalent versions.

Taking into account the fact that K3 does not interact with lysine-type zwitterionic ligands (Marti et al., 1994; Söhndel et al., 1996), the results presented here (Table 1) should help close the case for the location of the low-, intermediate-, and high-affinity binding sites in HPg (Markus et al., 1979).

REFERENCES

Arni, R. K., Padmanabhan, K., Padmanabhan, K. P., Wu, T.-P., & Tulinsky, A. (1993) *Biochemistry 32*, 4727−4737.

Atkinson, R. A., & Williams, R. J. P. (1990) *J. Mol. Biol. 212*, 541−552.

Brooks, B. R., Bruccoleri, R. E., Olafson, B. D., States, D. J., Swaminathan, S., & Karplus, M. (1983) *J. Comput. Chem. 4*, 187−217.

Byeon, I.-J. L., & Llinás, M. (1991) *J. Mol. Biol. 222*, 1035−1051.

Cao, Y., Ji, R. W., Davidson, D., Schaller, J., Marti, D., Söhndel, S., McCance, S. G., O'Reilly, M. S., Llinás, M., & Folkman, J. (1996) *J. Biol. Chem. 271*, 29461−29467.

Cox, M., Schaller, J., Boelens, R., Kaptein, R., Rickli, E., & Llinás, M. (1994) *Chem. Phys. Lipids 67/68*, 43−58.

De Marco, A. (1977) *J. Magn. Reson. 26*, 527−528.

De Marco, A., Hochschwender, S. M., Laursen, R. A., & Llinás, M. (1982) *J. Biol. Chem. 257*, 12716−12721.

De Marco, A., Pluck, N. D., Bányai, L., Trexler, M., Laursen, R. A., Patthy, L., Llinás, M., & Williams, R. J. P. (1985) *Biochemistry 24*, 748−753.

De Marco, A., Petros, A. M., Laursen, R. A., & Llinás, M. (1987) *Eur. Biophys. J. 14*, 359−368.

de Vos, A. M., Ultsch, M. H., Kelley, R. F., Padmanabhan, K., Tulinsky, A., Westbrook, M. L., & Kossiakoff, A. A. (1992) *Biochemistry 31*, 270−279.

Forsgren, M., Råden, B., Israelsson, M., Larsson, K., & Hedén, L.-O. (1987) *FEBS Lett. 213*, 254−260.

Günzler, W. A., Steffens, G. J., Ötting, F., Kim, S.-M. A., Frankus, E., & Flohé, L. (1982) *Hoppe-Seyler's Z. Physiol. Chem. 363*, 1155−1165.

Hansen, A. P., Petros, A. M., Meadows, R. P., Nettesheim, D. G., Mazar, A. P., Olejniczak, E. T., Xu, R. X., Pederson, T. M., Henkin, J., & Fesik, S. W. (1994) *Biochemistry 33*, 4847−4864.

Hayes, M. L., & Castellino, F. J. (1979a) *J. Biol. Chem. 254*, 8772−8776.

Hayes, M. L., & Castellino, F. J. (1979b) *J. Biol. Chem. 254*, 8777−8780.

Hochschwender, S. M., Laursen, R. A., De Marco, A., & Llinás, M. (1983) *Arch. Biochem. Biophys. 223*, 58−67.

Hochuli, E., Bannwarth, W., Döbeli, H., Gentz, R., & Stüber, D. (1988) *Bio/Technology 6*, 1321−1325.

Kaptein, R., Boelens, R., Scheek, R. M., & van Gunsteren, W. F. (1988) *Biochemistry 27*, 5389−5395.

Kumar, A., Ernst, R. R., & Wüthrich, K. (1980) *Biochem. Biophys. Res. Commun. 95*, 1−6.

Lerch, P. G., Rickli, E. E., Lergier, W., & Gillessen, D. (1980) *Eur. J. Biochem. 107*, 7−13.

Li, X., Bokman, A. M., Llinás, M., Smith, R. A. G., & Dobson, C. M. (1994) *J. Mol. Biol. 235*, 1548−1559.

Llinás, M., De Marco, A., Hochschwender, S. M., & Laursen, R. A. (1983) *Eur. J. Biochem. 135*, 379−391.

Magnusson, S., Petersen, T. E., Sottrup-Jensen, L., & Claeys, H. (1975) in *Proteases and biological control* (Reich, E., Rifkin, D. B., & Shaw, E., eds) pp. 123−149, Cold Spring Harbor Laboratory Press, Plainview, NY.

Markus, G., Priore, R. L., & Wissler, F. C. (1979) *J. Biol. Chem. 254*, 1211−1216.

Marti, D., Schaller, J., Ochensberger, B., & Rickli, E. E. (1994) *Eur. J. Biochem. 219*, 455−462.

Mathews, I. I., Vanderhoff-Hanaver, P., Castellino, F. J., & Tulinsky, A. (1996) *Biochemistry 35*, 2567−2576.

McCance, S. G., & Castellino, F. J. (1995) *Biochemistry 34*, 9581−9586.

McCance, S. G., Menhart, N., & Castellino, F. J. (1994) *J. Biol. Chem. 269*, 32405−32410.

McMullen, B. A., & Fujikawa, K. (1985) *J. Biol. Chem. 260*, 5328−5341.

Menhart, N., Sehl, L. C., Kelley, R. F., & Castellino, F. J. (1991) *Biochemistry 30*, 1948−1957.

Menhart, N., Hoover, G. J., McCance, S. G., & Castellino, F. J. (1995) *Biochemistry 34*, 1482−1488.

Mikaelian, I., & Sergeant, A. (1992) *Nucleic Acids Res. 20*, 376.

Mikol, V., LoGrasso, P. V., & Boettcher, B. R. (1996) *J. Mol. Biol. 256*, 751−761.

Motta, A., Laursen, R. A., Llinás, M., Tulinsky, A., & Park, C. H. (1987) *Biochemistry 26*, 3827−3836.

Mulichak, A. M., Tulinsky, A., & Ravichandran, K. G. (1991) *Biochemistry 30*, 10576−10588.

Novokhatny, V. V., & Kudinov, S. A. (1984) *J. Mol. Biol. 179*, 215−232.

O'Reilly, M. S., Holmgren, L., Shing, Y., Chen, C., Rosenthal, R. A., Moses, M., Lane, W. S., Cao, Y., Sage, E. H., & Folkman, J. (1994) *Cell 79*, 315−328.

Pennica, D., Holmes, W. E., Kohr, W. J., Harkins, R. N., Vehar, G. A., Ward, C. A., Bennett, W. F., Yelverton, E., Seeburg, P. H., Heyneker, H. L., & Goeddel, D. V. (1983) *Nature 301*, 214−221.

Petros, A. M., Gyenes, M., Patthy, L., & Llinás, M. (1988) *Arch. Biochem. Biophys. 264*, 192−202.

Petros, A. M., Ramesh, V., & Llinás, M. (1989) *Biochemistry 28*, 1368−1376.
Ramesh, V., Petros, A. M., Llinás, M., Tulinsky, A., & Park, C. H. (1987) *J. Mol. Biol. 198*, 481−498.
Rejante, M. R. (1992) Ph.D. Dissertation, Carnegie Mellon University, Pittsburgh, PA.
Rejante, M. R., & Llinás, M. (1994a) *Eur. J. Biochem. 221*, 939−949.
Rejante, M. R., & Llinás, M. (1994b) *Eur. J. Biochem. 221*, 927−937.
Rejante, M. R., Byeon, I.-J. L., & Llinás, M. (1991) *Biochemistry 30*, 11081−11092.
Rosenberg, A. H., Lade, B. N., Chui, D.-S., Lin, S.-W., Dunn, J. J., & Studier, F. W. (1987) *Gene 56*, 125−135.
Söhndel, S., Hu, C.-K., Marti, D., Affolter, M., Schaller, J., Llinás, M., & Rickli, E. E. (1996) *Biochemistry 35*, 2357−2364.
Sottrup-Jensen, L., Claeys, H., Zajdel, M., Petersen, T. E., & Magnusson, S. (1978) *Prog. Chem. Fibrinolysis Thrombolysis 3*, 191−209.
Stanssens, P., Opsomer, C., McKeown, Y. M., Kramer, W., Zabeau, M., & Fritz, H.-J. (1989) *Nucleic Acids Res. 12*, 4441−4453.
Studier, F. W., Rosenberg, A. H., Dunn, J. J., & Dubendorff, J. W. (1990) *Methods Enzymol. 185*, 60−89.
Thewes, T., Ramesh, V., Simplaceanu, E. L., & Llinás, M. (1987) *Biochim. Biophys. Acta 912*, 254−269.
Thewes, T., Constantine, K., Byeon, I.-J. L., & Llinás, M. (1990) *J. Biol. Chem. 265*, 3906−3915.
Tulinsky, A., Park, C. H., Mao, B., & Llinás, M. (1988a) *Proteins: Struct., Funct., Genet. 3*, 85−96.
Tulinsky, A., Park, C. H., & Skrypczak-Jankun, E. (1988b) *J. Mol. Biol. 202*, 885−901.
Wider, A., Macura, S., Kumar, A., Ernst, R. R., & Wüthrich, K. (1984) *J. Magn. Reson. 56*, 207−234.
Wiman, B. (1977) *Eur. J. Biochem. 76*, 129−137.
Wu, T.-P., Padmanabhan, K., Tulinsky, A., & Mulichak, A. M. (1991) *Biochemistry 30*, 10589−10594.
Wu, T.-P., Padmanabhan, K., & Tulinsky, A. (1994) *Blood Coagulation Fibrinolysis 5*, 157−166.

BI971316V